PERGAMON

International Journal of Heat and Mass Transfer 44 (2001) 1725–1734

International Journal of HEAT and MASS TRANSFER

www.elsevier.com/locate/ijhmt

Temperature-dependent thermal lagging in ultrafast laser heating

D.Y. Tzou *, K.S. Chiu

Department of Mechanical and Aerospace Engineering, University of Missouri – Columbia, Columbia, MO 65211, USA

Received 7 January 2000; received in revised form 16 June 2000

Abstract

Temperature-dependent phase-lags are incorporated in the dual-phase-lag (DPL) model to fully describe the experimental data of femtosecond (fs) laser heating on gold films of various thicknesses in the sub-micron range. An explicit finite difference algorithm is developed to perform the nonlinear analysis, which recovers the Crank–Nicholson stability criterion in the special case of Fourier diffusion. The exponents in the temperature-dependent thermal properties are determined by minimizing the mean error between the numerical and the experimental results. The lagging model with temperature-dependent thermal properties enables a consistent description of all the available experimental data for ultrafast laser heating on gold films.

1. Introduction

The unique capability of short-pulse lasers lies in its high-precision control of heating times and locations in thermal processing of materials. Due to the short duration in local heating, the short-pulse energy deposition effectively confines the heat-affected zone within the pre-designed physical domain, resulting in well-controlled thermal processes, such as the localized phase change and constituents, doping in metallic films and bond-tailoring for applications to microbiological tissues. Developments of the high-power short-pulse lasers have matured into several innovative technologies, including structural monitoring of thin metal films [1,2], laser micro-machining [3] and patterning [4], structural tailoring of microfilms [5], and laser synthesis and processing in thin-film deposition [6]. In addition to the development of new technologies, most importantly, the femtosecond (fs) laser has become an effective tool for investigating the fundamental process of heat transport in micro-scale [7–12]. The theoretically derived and experimentally verified phonon–electron coupling factor for metal films, for example, has placed the hypothetical microscopic two-step model [13,14] on a firm physical basis. The thermal lagging model describing the picosecond (ps) heat transport in metal films [15–19], as another example, has introduced two phase-lags whose engineering values must be determined from the experimental data employing the fs lasers. While more aggressive applications are attempted and new physical models are developed for describing heat transport in different micro-systems, the role that high-power short-pulse lasers play in advanced technologies is expected to grow drastically.

During ultrafast heating on metallic films, the temperature change is converted from the reflectivity change measured optically on the film surfaces [7–12]. Due to much smaller heat capacity of the electron gas than the metal lattice, the temperature rise during the first few ps is mainly caused by the hot electron gas rather than the metal lattice. Major focus in modeling the ultrafast process of heat transport, therefore, has been placed on the electron gas whose temperature becomes physically meaningful after the first few hundred femtoseconds [9–12]. Development of the microscopic two-step model is an example at hand. Optically, the maximum reflectivity change varies linearly with laser fluence. The maximum temperature rise of the electrons, in addition, is almost proportional to laser fluence in the heating history. In

* Corresponding author. Tel.: +1-573-882-4060; fax: +1-573-884-5090.

E-mail address: tzour@missouri.edu (D.Y. Tzou).

0017-9310/01/$ - see front matter
PII: S0017-9310(00)00215-5

Nomenclature

C	volumetric heat capacity [J m^{-3} K^{-1}]
C_{cv}	Cattaneo–Vernotte thermal wave speed [m s^{-1}]
E	mean error of the normalized temperature change, dimensionless
G	phonon–electron coupling factor [W m^{-3} K^{-1}]
J	laser fluence [J m^{-2}]
k	thermal conductivity [W m^{-1} K^{-1}]
L	film thickness [m]
M	exponent, dimensionless
N	exponent, dimensionless
P	exponent, dimensionless
q	one-dimensional heat flux [W m^{-2}]
R	reflectivity, dimensionless
S	energy absorption rate [W m^{-3}]
T	temperature [K]
T_0	initial temperature [K]
U	exponent, dimensionless
t	physical time [s]
x	space variable [m]

Greek symbols

α	thermal diffusivity [m^2 s^{-1}]
δ	laser penetration depth [m]
η	amplification factor for heat flux [W^n m^{-2n}]
κ	wave number [m^{-1}]
τ	phase lag [s]
ξ	amplification factor for temperature [K$^{1/n}$]

Subscripts and superscript

e	electron
exp	experimental
j	nodal number of the spatial grid
l	lattice
max	maximum value
n	nodal number of the time grid
num	numerical
p	pulse
q	heat flux vector
T	temperature gradient
0	reference state

modeling the temperature change in the electron gas (T_e), therefore, the normalized reflectivity change (with respect to its maximum value) is assumed to be proportional to the normalized temperature change of electrons. For an ultrafast heating on metal films, such a proportional relation holds as long as the electron temperature is lower than the Debye temperature. Based on this assumption, in fact, the phonon–electron coupling factor (G), an intrinsic thermal property characterizing the ultrafast thermal energy exchange between electrons and phonons, was determined for nine metallic elements [9]. The dual-phase-lag model (DPL) [15–19], alternatively, describes the thermal relaxation and thermalization behaviors that are interweaving in the ultrafast process of heat transport in the electron gas. Two intrinsic delay times, called phase-lags denoted by τ_T and τ_q, were introduced to account for the finite times required for the thermal equilibrium (τ_T) and effective collisions (τ_q) between electrons and phonons to take place

$$\begin{aligned} q(r,t+\tau_q) &= -k\nabla T(r,t+\tau_T)_{\text{first-order model}} \\ &\Rightarrow q(r,t)+\tau_q\frac{\partial q}{\partial t}(r,t) \\ &= -k\left[\nabla T(r,t)+\tau_T\frac{\partial}{\partial t}\nabla T(r,t)\right]. \end{aligned} \tag{1}$$

In relation to the micro-structural parameters in the parabolic two-step (PTS) model, at a constant temperature

$$\tau_T=\frac{C_l}{G},\quad \tau_q=\frac{1}{G}\left(\frac{1}{C_e}+\frac{1}{C_l}\right)^{-1}. \tag{2}$$

Similar correlations of τ_T and τ_q exist when describing different behaviors of energy carriers in different types of conductors. In terms of the two lagging times, to date, the DPL model has described seven microscopic and macroscopic models in the same framework of thermal lagging [18,19]. They include the hyperbolic two-step models for metals [10], the phonon scattering model for insulators, semiconductors and dielectric films [20], the three-equation model describing the additional thermal relaxation of internal energy [21], heat transport in amorphous media [22] and, of course, the classical CV-wave model [23,24]. Instead of tracking different micro-structural interactions in different types of conductors, the phase-lag concept focuses attention on the finite times that are required for the various micro-structural interactions to take place. In fact, evidenced by the existence of the thermalization time and the relaxation time in the phonon–electron interaction model and the normal and umklapp relaxation times in the phonon scattering model, such a time-concept has already been implied. The characteristic times governing the various physical processes of energy transport can be derived in the various micro-scale models, but the DPL model implements these characteristic times in a concise fashion. The correlations of τ_T and τ_q to the various micro-structural parameters, exemplified by Eq. (2) in correlation to the phonon–electron interaction model, are to extract the physical source for time delays from the various physical processes in micro-scale. During the phonon–electron interactions, the phonon–electron coupling factor (G) stands for the energy exchange

between phonons and electrons per unit volume per unit time. Heat flow arrives at such a compound system at time t. The temperature gradient, across the same volume, can only be established later, at $t+\tau_T$, because it requires a finite duration, $\tau_T = C_l/G$, to raise the temperature of the metal lattice (with the heat capacity per unit volume being C_l) by one degree. Heat flow leaves the compound system at time $t+\tau_q$, after another finite duration, $\tau_q = (1/C_e + 1/C_l)^{-1/G}$, which is required for effective collisions between phonons and electrons to take place for heat transport. Clearly, a parallel assembly is assumed between the electrons and the phonons, and the phase lag τ_q refers to the finite time required to raise the temperature of the compound system (with the effective heat capacity per unit volume being $(1/C_e + 1/C_l)^{-1}$) by one degree. Allocating τ_T to address the delay behavior in establishing the temperature gradient and τ_q to address the delay behavior in heat-flow departure is a unique feature in the DPL model, which has been supported by the successful correlations to seven microscopic models as well as a rigorous derivation in the framework of the nonequilibrium and irreversible thermodynamics [18].

The concept of temperature employed in all the microscopic models, including the DPL model, may have a different context from the one defined on the basis of thermal equilibrium. Especially during the sub-ps transient in metals where thermal equilibrium remains distant, the temperature used in these models may only refer to a fast-varying thermal disturbance propagating in the conducting system. Although, numerous efforts have been made to distinguish the nonequilibrium temperature from the local-equilibrium temperature [18,25], the nonequilibrium temperature remains to be defined in an operational sense. In the absence of a device that is sufficiently fast to measure the "temperature" directly in the domain of ps, in fact, relating the normalized temperature *change* to the directly measured normalized reflectivity change is a unique contribution of the recent development of the microscopic two-step model [7–12]. In this regard, the change of temperature may be a more physical index than the temperature itself to measure the strength of the thermal disturbance in ultrafast heating.

The two phase-lags, τ_T and τ_q, are central quantities in Eq. (1) that replace the classical Fourier's law in coupling with the energy equation. For gold, their effective values averaging over a nominal range of temperature were determined as $\tau_T = 90$ ps and $\tau_q = 8.5$ ps [18]. These values, however, aim to describe the overall behavior of thermal lagging during the ps transient, but reveal no detailed variations of phase-lags with temperature. As a result, significant deviations may result when using these values in predicting the rear-surface temperature or surface temperatures in general for thinner films. This work aims to broaden the analysis by accommodating the temperature-dependent thermal properties in describing the ultrafast process of heat transport in metal films. The problem becomes highly nonlinear due to the temperature-dependent lagging behavior, necessitating a numerical study of the fast transient phenomena. An explicit finite difference algorithm shall be developed to quantify the lagging temperature developed at short times. It employs a mixed formulation, specially tailored to recover the Crank–Nicholson stability criterion in Fourier's law as the lagging behavior diminishes. With the temperature dependency thus incorporated, it will be shown that the DPL model accurately describes the available experimental data for ultrafast heating on gold films of various thicknesses.

2. Ultrafast heating on metals

Fs laser heating has been modeled by the energy absorption rate in the thin film [9–12,17–19]. As the film thickness is of the order of sub-microns in most cases, which is much smaller than the characteristic dimension of the laser-heated spot, in addition, the one-dimensional formulation has been adopted in analyzing the ultrafast processes of thermal relaxation and thermalization. The DPL model shown by Eq. (1) can be reduced to

$$q(x,t) + \tau_q(T)\frac{\partial q}{\partial t}(x,t) = -k(T)\left[\frac{\partial T}{\partial x}(x,t) + \tau_T(T)\frac{\partial^2 T}{\partial x\,\partial t}(x,t)\right] \tag{3}$$

in this case, which is to be coupled with the one-dimensional energy equation

$$-\frac{\partial q}{\partial x}(x,t) + S(x,t) = C(T)\frac{\partial T}{\partial t}(x,t) \tag{4}$$

to describe the temperature (T) and heat flux (q) distributions in the thickness (x)-direction of the film. Thermal conductivity (k), volumetric heat capacity (C), phase-lag of the temperature gradient (τ_T), and phase-lag of the heat flux vector (τ_q) in Eq. (4) are functions of temperature during the heating process. In contrast to the two-step model, where separate equations are used for describing the individual temperatures of the electron gas and the metal lattice [9–12], Eq. (4) describes the electron temperature alone with effect of phonon coupling absorbed in the *effective* thermal properties k, C, τ_T and τ_q [15–19]. Thermal properties of the metal lattice have definite influences on the two phase-lags, exemplified by Eq. (1) at a constant temperature. Effective heat capacity results from the serial assembly of electrons and phonons, $C = C_e + C_l$, while thermal conductivity (k) remains to be that of the electrons since conduction effect through the sub-micron thickness is neglected in the metal lattice.

The energy absorption rate, $S(x,t)$, results from the rather complicated beam–material interaction [15,18]

$$S(x,t)=0.94J\left(\frac{1-R}{t_p\delta}\right)\exp\left(-\frac{x}{\delta}-\frac{1.992|t-2t_p|}{t_p}\right). \quad (5)$$

The time exponential replaces the Gaussian distribution employed by Qiu and Tien [9], with the constant 1.992 determined from the normalized autocorrelation function of the 96 fs laser pulse ($t_p = 96$ fs) [15,17–19]. The initial time is shifted to $-2t_p$ to reflect the full width at half maximum (FWHM) pulse duration, with the energy absorption rate now peaking at time zero.

The effective phase-lags (τ_T and τ_q) and volumetric heat capacity ($C = C_e + C_l$) in the DPL model can be calculated exactly from Eq. (2) at a constant temperature. For gold at room temperature, $T_0 = 300$ K, for example, $C_e = 2.1\times10^4$ J m^{-3} K^{-1}, $C_l = 2.5\times10^6$ J m^{-3} K^{-1}, and $G = 2.8\times10^{16}$ W m^{-3} K^{-1} [9], which result in $\tau_{T0} = 89.286$ ps, $\tau_{q0} = 0.7438$ ps, and $C_0 = 2.5\times10^6$ J m^{-3} K^{-1} ($\cong C_l$, since C_e is smaller than C_l by two orders of magnitude). Comparing to the averaged values of $\tau_T = 90$ ps and $\tau_q = 8.5$ ps over a nominal range of temperature [15,18,19], the value of τ_T remains approximately the same while the value of τ_q at room temperature is lower by approximately one order of magnitude. Temperature dependence of the effective thermal properties needs to be modeled in detail as the film temperature significantly varies in high-power laser heating. For this purpose, we assume the following polynomial forms:

$$\begin{aligned}&\tau_T(T)=\tau_{T0}\left(\frac{T}{T_0}\right)^M, \quad \tau_q(T)=\tau_{q0}\left(\frac{T}{T_0}\right)^N,\\ &k(T)=k_0\left(\frac{T}{T_0}\right)^P, \quad C(T)=C_0\left(\frac{T}{T_0}\right)^U,\end{aligned} \quad (6)$$

where the exponents M, N, P, and U are to be determined by minimizing the mean error between the numerical and the experimental results.

Two boundary conditions and two initial conditions are required to solve the temperature and heat flux from Eqs. (3) and (4), which are called the mixed formulations in the DPL model. Due to the complicated relationship between the temperature and the heat flux vector in thermal lagging, as shown by Eq. (3), the mixed formulation is particularly useful for problems involving flux-specified boundary conditions. No energy loss is expected to occur from the film surface during the ps transient. Consequently, the insulated boundary conditions are imposed at both the front ($x = 0$) and rear ($x = L$) surfaces of the film:

$$q = 0 \quad \text{at } x = 0 \quad \text{and} \quad x = L. \quad (7)$$

The initial temperature, at $t = 2t_p$, is assumed to be T_0, while no heat flow exists prior to laser heating

$$T = T_0 \quad \text{and} \quad q = 0 \quad \text{at } t = -2t_p. \quad (8)$$

3. Finite differencing

Temperature dependency shown by Eq. (6) introduces strong nonlinearity into the problem, Eqs. (3)–(5) subjected to the boundary and initial conditions in Eqs. (7) and (8). A special finite difference algorithm has been developed to solve the nonlinear problem [25]. The backward difference in space is first applied to the first-order derivatives with respect to x in Eqs. (3) and (4):

$$\left(\frac{\partial T}{\partial x}\right)_j^n \cong \frac{T_j^n - T_{j-1}^n}{\Delta x}, \quad \left(\frac{\partial q}{\partial x}\right)_j^n \cong \frac{q_j^n - q_{j-1}^n}{\Delta x}. \quad (9)$$

The *backward* difference, in time, is then applied to the mixed-derivative term, $(\partial^2 T/\partial x\,\partial t)$, and $(\partial q/\partial t)$ in Eq. (3)

$$\left(\frac{\partial^2 T}{\partial x\,\partial t}\right)_j^n = \frac{T_{j+1}^n - T_{j-1}^n - T_{j+1}^{n-1} + T_{j-1}^{n-1}}{2\Delta x\,\Delta t}. \quad (10)$$

The first-order derivative of temperature with respect to time, $(\partial T/\partial t)$ in Eq. (4), at last, is approximated by the *forward* difference in time

$$\left(\frac{\partial T}{\partial t}\right)_j^n = \frac{T_j^{n+1} - T_j^n}{\Delta t}. \quad (11)$$

Substituting Eqs. (9)–(11) into Eqs. (3) and (4) renders two finite difference equations to be solved for the two unknowns, T_j^n and q_j^n. The stability and convergence criteria for this algorithm can be obtained by performing the von Neumann eigenmode analysis [26,27]. Assuming the error propagation modes for the lagging temperature and heat flux in the following form:

$$\begin{aligned}&T_j^n = \xi^n \exp[\imath\kappa(j\Delta x)],\\ &q_j^n = \eta^n \exp[\imath\kappa(j\Delta x)] \quad \text{with} \quad \imath = \sqrt{-1}\end{aligned} \quad (12)$$

the two difference equations can be solved explicitly for the amplification factors ξ and η. To ensure stable and convergent solutions of T_j^n and q_j^n, it is required that $|\xi| < 1$ and $|\eta| < 1$, which can be combined and simplified to give

$$\Delta x \geqslant \sqrt{\frac{2\alpha\Delta t\,(2\tau_T + \Delta t)}{2\tau_q + \Delta t}}. \quad (13)$$

Under a prescribed time increment (Δt), Eq. (13) dictates the minimum space increment (Δx) that must be followed to achieve the stable and convergent solutions according to the finite difference algorithm described in Eqs. (9) and (11). In the case of Fourier diffusion, $\tau_T = \tau_q$ [15,18], obviously, Eq. (13) reduces to the familiar Crank–Nicholson stability criterion. In the case of $\tau_T = 0$, as another example, Eq. (13) reduces to

$$\frac{\Delta x}{(C_{cv}\Delta t)}\frac{1}{\sqrt{1+(1/2)(\Delta t/\tau_q)}} \quad \text{with} \quad C_{cv} = \sqrt{\frac{\alpha}{\tau_q}} \quad (14)$$

which is the stability and convergence criteria for the thermal wave model in the present scheme, with C_{cv} standing for the finite speed of heat propagation.

At time $t = n\Delta t$, the thermal properties in Eqs. (3) and (4) are calculated from the temperature obtained at the previous time, $t = (n-1)\Delta t$. The finite difference form of the term $\tau_q(T)\partial q/\partial t$ in Eq. (3), for example, is

$$\left[\tau_q(T)\frac{\partial q}{\partial t}\right]_j^n = \left[\tau_{q0}\left(\frac{T}{T_0}\right)^N\right]_j^n \left[\frac{\partial q}{\partial t}\right]_j^n \cong \tau_{q0}\left(\frac{T_j^{n-1}}{T_0}\right)^N \left(\frac{q_j^n - q_j^{n-1}}{\Delta t}\right). \quad (15)$$

The initial values of τ_{T0}, τ_{q0}, k_0 and C_0 (at $T = T_0$) are used for calculating the temperature distribution at $t = \Delta t$. The new temperatures are then used to calculate the new values of thermal properties at each node according to Eq. (6), based on which the calculation is advanced to $t = 2\Delta t$. This procedure continues until the prescribed final time is arrived. In each time step, based on the updated value of α ($\equiv k/C$), the minimum space increment is calculated at each node according to Eq. (13). Maximum in these minimum increments is then selected as the space increment to assure a global satisfaction of the stability and convergence criteria.

Accuracy of the finite difference calculations performed in this work is ensured by continuous halving of the time increment, and, consequently, adjusting the space increment according to Eq. (13), until a uniform convergence of the numerical solutions are achieved for both temperature and heat flux. The results shown below employ the value of $\Delta t = 0.85$ fs, resulting in a space increment of the order of 5 nm, depending on the local temperatures established during the short-time transient. The Cauchy norm between successive halving is less than one percent in all cases.

4. Numerical results

The finite difference scheme described in Eqs. (9)–(11) and the stability criterion established in Eq. (13) are first examined by the analytical solution for gold with constant effective thermal properties, $\alpha = 1.2\times 10^{-4}$ m^2 s^{-1}, $k = 315$ W m^{-1} K^{-1}, $\tau_T = 90$ ps, and $\tau_q = 8.5$ ps [18]. The results are displayed in Fig. 1, along with the experimental results obtained in [8,12]. At the front surface ($x = 0$) of a 0.1 μm gold film, the temperature change is normalized by the maximum value that occurs during the short-time transient. The resulting normalized temperature change is proportional to the normalized surface reflectivity measured directly in the experiments. For $\Delta t = 0.85$ fs, the finite difference results are obtained by the use of $\Delta x = 5$ nm, which satisfies the stability criteria shown by Eq. (13),

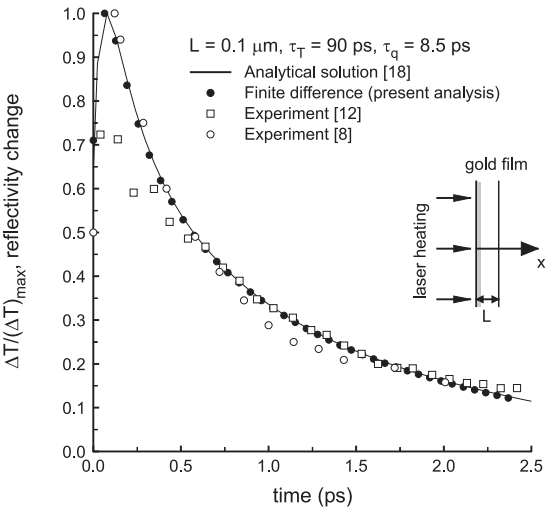

Fig. 1. Normalized temperature change at the front surface of a gold film of thickness 0.1 μm: $\alpha = 1.2\times 10^{-4}$ m^2 s^{-1}, $k = 315$ W m^{-1} K^{-1}, $\tau_T = 90$ ps, $\tau_q = 8.5$ ps, and $\Delta x = 5$ nm in the finite difference result.

$\Delta x \geqslant 4.947$ nm. The finite difference results agree very well with the analytical result obtained by the Riemann-sum approximation, justifying the accuracy of the finite difference scheme developed in Eqs. (9)–(11) and the stability and convergence criteria shown by Eq. (13).

Temperature-dependent thermal properties: The DPL model with constant phase-lags is able to describe the temperature change at the front surface of the 0.1 and 0.2 μm gold films [15,17–19]. For describing the temperature changes at the rear surfaces, as well as the surface temperatures in gold films of other thicknesses, however, refined mechanisms such as the temperature dependence of thermal properties on the heating history need to be included [15]. A consistent description developed in this fashion necessitates the determination of the exponents M, N, P and U shown in Eq. (6), and the extended use of their same values for gold films of the various thicknesses.

The normalized temperature changes at the front surface ($x = 0$) of the 0.1 μm film are used to define the mean error between the numerical and the experimental results in [12]

$$E(M,N,P,U) = \frac{\sum_{n=1}^{\aleph}\left[\left(\frac{\Delta T(x=0,t=t_n;M,N,P,U)}{\Delta T_{max}}\right)_{num} - \left(\frac{\Delta T(x=0,t=t_n)}{\Delta T_{max}}\right)_{exp}\right]}{\aleph}, \quad (16)$$

where t_n refer to the n-instants of time at which the experimental results are extracted, $\aleph$ denotes the total number of data points taken for comparisons, and the

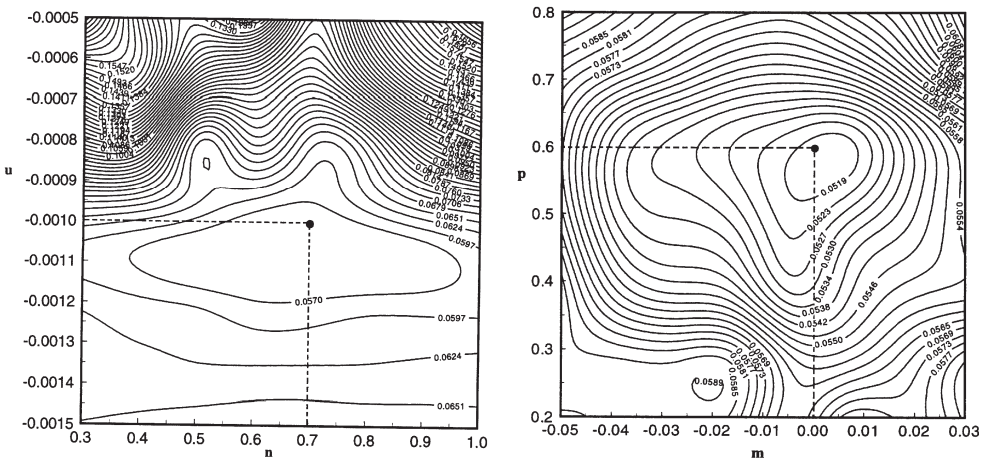

(a) *NU*-space (b) *MP*-space

Fig. 2. Minimum values of the mean error E at: (a) $(N, U) = (0.7, -0.001)$ for $M = 0$ and $P = 0.6$; (b) $(M, P) = (0, 0.6)$ for $N = 0.7$ and $U = -0.001$.

quantity $(\Delta T/(\Delta T)_{\max})_{\exp}$ is indeed $(\Delta R/(\Delta R)_{\max})$ because the directly measured quantity in the experiments is the change of the surface reflectivity. Since the temperature of the electron gas possesses a deterministic physical meaning after the first few hundred femtoseconds, a total of 19 data points (and hence $n = 19$) is selected from the experimental curve [12] in Fig. 1 after $t > 0.6$ ps (600 fs). The numerical results, and, consequently, the mean error, depend on the values of M, N, P and U that are selected in the numerical computations. The desirable values of M, N, P and U should minimize the mean error E [18], and consequently render a small difference between the numerical and the experimental results in an overall sense

$$\frac{\partial E}{\partial M} = 0, \quad \frac{\partial E}{\partial N} = 0, \quad \frac{\partial E}{\partial P} = 0, \quad \frac{\partial E}{\partial U} = 0. \tag{17}$$

From an analytical point of view, Eq. (17) provides four equations to be solved for the four parameters M, N, P and U. Numerically, fine grids for M, N, P and U are prepared to approximate the first-order derivatives shown in Eq. (17), resulting in the threshold values of $M = 0, N = 0.7, P = 0.6$, and $U = 0.001$ for gold

$$\begin{aligned} &\tau_T(T) = \tau_{T0}, \quad \tau_q(T) = \tau_{q0}\left(\frac{T}{T_0}\right)^{0.7}, \\ &k(T) = k_0\left(\frac{T}{T_0}\right)^{0.6}, \quad C(T) = C_0\left(\frac{T}{T_0}\right)^{-0.001}. \end{aligned} \tag{18}$$

Fig. 2 shows the typical contour patterns of E in the U–N and P–M spaces that illustrate the minima of E at these values. The phase-lag of the temperature gradient, τ_T, appears to be temperature-independent (constant), which is supported by Eq. (2) since the phonon–electron coupling factor (G) and volumetric heat capacity of the metal lattice (C_l) are temperature insensitive. The effective volumetric heat capacity, $C = C_e + C_l$, in addition, turns out to be a weak function of temperature as the exponent –0.001 is close to zero. This behavior is also supported by Eq. (2) as the volumetric heat capacity of the electron gas (C_e) is approximately two orders of magnitude smaller than that of the metal lattice (C_l), and the value of C_l is much less temperature-dependent than that of C_e [9]. These arguments, to repeat, can only be viewed approximate because Eq. (2) is only valid at a constant temperature.

Extended applications: Eq. (18) determined from the experimental results at the *front* surface of a 0.1 μm gold film is used in the DPL model to examine the temperature changes in gold films of different thicknesses, at

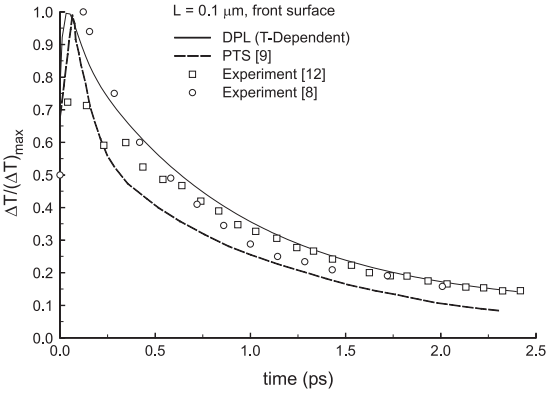

Fig. 3. Normalized temperature change at the front surface of a 0.1 μm gold film.

both the front and *rear* surfaces where experimental data are available in [8,12]. Since Eq. (18) describes the intrinsic properties of gold films, it shall be consistently used for all the film thickness under consideration.

Fig. 3 shows the normalized temperature change at the front surface ($x = 0$) of a 0.1 μm gold film, calculated by the finite difference scheme Eqs. (9)–(11) and Eq. (13)) with the temperature-dependent thermal properties shown in Eq. (18). The finite difference results agree well with the experimental data in rapid thermalization, $t > 0.6$ ps. The DPL model with temperature-dependent thermal properties is comparable to the parabolic two-step (PTS) model addressing the temperature-dependent heat capacity of the electron gas [9]. Of the same thickness (0.1 μm) but at the *rear* surface ($x = 0.1$ μm), Fig. 4 shows the normalized temperature changes in comparison with the experimental data. Satisfactory agreement is reproduced, which is considered a great improvement because the DPL model assuming *constant* effective properties encountered difficulties in interpreting the experimental data at the rear surface of the film [18].

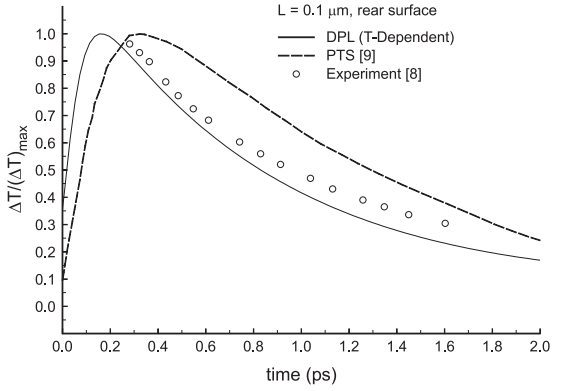

Fig. 4. Normalized temperature change at the rear surface of a 0.1 μm gold film.

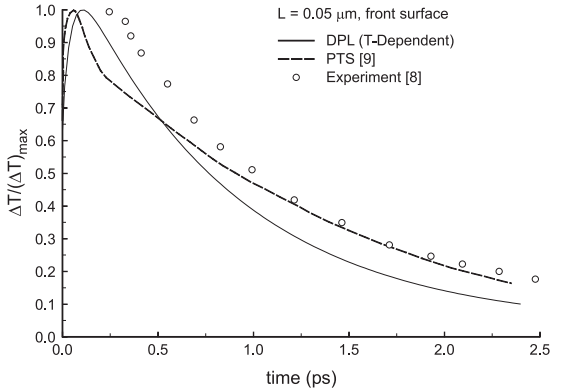

Fig. 5. Normalized temperature change at the front surface of a 0.05 μm gold film.

Employing the same temperature-dependent thermal properties, Eq. (18), Figs. 5 and 6 show the normalized temperature change calculated at the front ($x = 0$) and

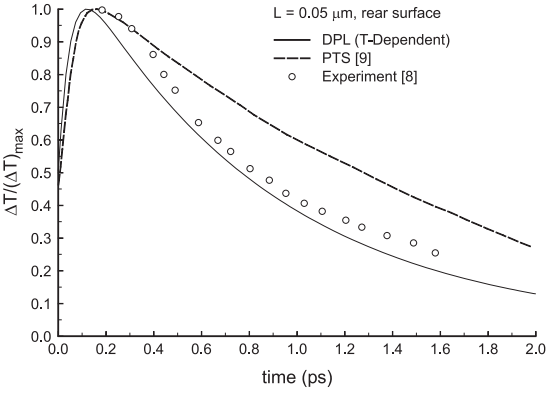

Fig. 6. Normalized temperature change at the rear surface of a 0.05 μm gold film.

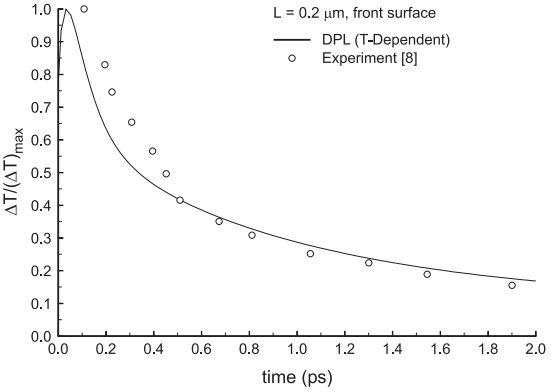

Fig. 7. Normalized temperature change at the front surface of a 0.2 μm gold film.

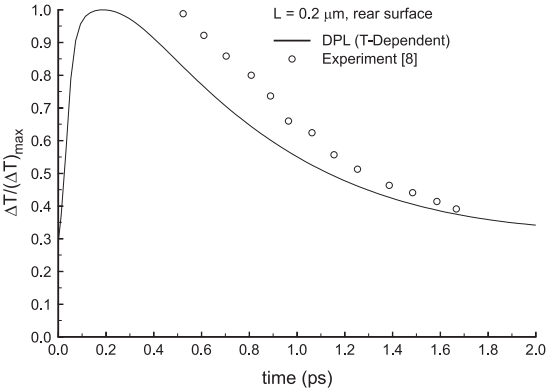

Fig. 8. Normalized temperature change at the rear surface of a 0.2 μm gold film.

rear ($x = 0.05$ μm) surfaces of a thinner gold film, $L = 0.05$ μm. Although a larger deviation is observed at the front surface, the normalized temperature changes predicted by the DPL model are well within the threshold of experimental uncertainties [8]. The normalized temperature changes predicted by the DPL model for a thicker gold film of $L = 0.2$ μm are displayed in Figs. 7 and 8. Again, a consistent use of Eq. (18) describing the temperature-dependent thermal properties in DPL gives satisfactory results in comparing with the experimental data at both the front and rear surfaces.

Rapid thermalization and relaxation result in a more uniform temperature distribution in a thinner film, as shown by Fig. 9 where the interior temperature changes in each case are normalized with respect to the corresponding maximum value occurring at the front surface, $\Delta T/(\Delta T)^0_{\max} \equiv \Delta T/(\Delta T)_{\max}$ at $x = 0$. The temperatures at different locations are close in the 0.05 μm gold film, Fig. 9(a), with the peaking time slightly increasing with the distance from the front surface (a larger value of x). The same trend is preserved for temperature changes in a thicker film, as shown in Fig. 9(b) with $L = 0.1$ μm. A larger physical domain enhances the transport process of phonon–electron relaxation, and hence there is a more pronounced lagging behavior, as reflected by the larger temperature gradient existing in the thickness direction. The peaking time also increases in the direction towards the rear surface of the film, which is more obvious than that shown in Fig. 9(a) in a thinner film.

5. Conclusion

The temperature-dependent thermal properties, including the phase-lags describing the lagging behavior in ultrafast heat transport, have been incorporated in the DPL model for a consistent description of the thin-film transient reflectivity. The temperature dependence is determined by minimizing the mean error between the numerical and experimental results of the normalized temperature changes at the front surface of a 0.1 μm gold film heated by a 96 fs laser. The temperature-dependent thermal properties thus determined are used consistently to determine the normalized temperature changes at both the front and rear surfaces of 0.05, 0.1, and 0.2 μm gold films. Rigorous examinations show that the normalized temperature changes predicted by the DPL model agree well with the experimental results, supporting the temperature-dependent lagging behavior in ultrafast laser heating on metal films. In accuracy, the DPL model accommodating the temperature-dependent thermal properties is comparable to the parabolic two-step model established on a different physical basis. The complicated phonon–electron interaction in space, alternatively, may be interpreted in terms of the lagging behavior in time. Thermal properties are determined in the present work by minimizing the mean errors between the model and the experimental results, which is in essence an inverse analysis [28]. The level of agreements shown in Figs. 3–8 already lies within the uncertainties (15–20%) in this type of experiments, although the use of mean square error may further improve the accuracy in

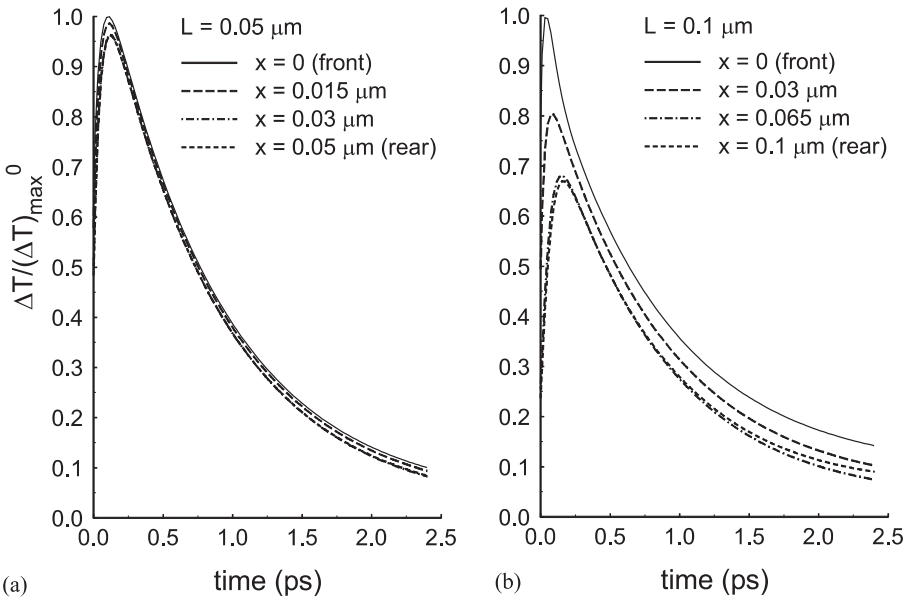

Fig. 9. Normalized temperature changes in the interior of the gold film: (a) $L = 0.05$ μm; (b) $L = 0.1$ μm.

describing the experimental curves. Such an inverse analysis should not be confused with the curve fitting routines. To accurately describe the transient response in gold films of different thicknesses and surfaces, most importantly, the type of differential equations (describing energy transport) must be correct that properly accommodates the thermalization and the relaxation behaviors during the ultrafast transient. The two phase-lags, τ_T and τ_q, appear as the coefficients in front of the highest order differentials in the DPL equation, which consequently dictate the fundamental behavior of the lagging response. Should the DPL equation be incorrect in describing the fast transient response in gold films, adjusting their (τ_T and τ_q) values in the DPL equation will not impel closer agreements with the experimental results. The agreement shown in this work, therefore, should not be viewed as a result of having more parameters involved in the DPL model to "fit" the experimental data. This can be further elaborated by considering the use of the CV-wave equation to interpret an experimentally obtained smooth curve. A sharp wavefront will always exist in the transient solution of the CV-waves, regardless of the value of the relaxation time chosen in the CV-wave equation. Although the CV-wave model has one more parameter, namely the relaxation time, than the Fourier's diffusion equation, in other words, it can never predict a smooth curve unless the transient time becomes much longer than the preset relaxation time.

The stability and convergence criteria derived on the basis of the mixed formulation is another feature in the present work. These criteria can be extended to cover a wide class of problems in microscale heat transport since the DPL equation is in a general form that captures seven different types of energy equations in special cases. As different values of τ_T, τ_q, and α are taken from the relations to the various microscopic properties in other models, different forms of the criteria are generated as a natural consequence. The stability and convergence criteria presented in this work for the Fourier diffusion and CV-wave models are typical examples.

The finite difference analysis provided in this work facilitates a direct study of multi-dimensional effects in thin-film heating. Thermal lagging around microvoids or sharp edges, and the resulting intensifications in the near filed, for example, are refined mechanisms to be further quantified. This is an ongoing effort in the development of the DPL model.

References

[1] J. Opsal, The application of thermal wave technology to thickness and grain size of aluminum films, in: Metallization: Performance and Reliability Issues for VLSI and ULSI, SPIE 1596 (1991) 120–131.

[2] A. Mandelis, S.B. Peralta, Thermal-wave based materials characterization and nondestructive evaluation of high-temperature superconductors: a critical review, in: R. Kossowsky (Ed.), Physics and Materials Science of High Temperature Superconductors II, Kluwer Academic Publishers, Boston, Massachusetts, 1992, pp. 413–440.

[3] J.A. Knapp, P. Børgesen, R.A. Zuhr (Eds.), Beam–solid interactions: physical phenomena. Mater. Res. Soc. Symp. Proc. vol. 157, Materials Research Society, Pittsburgh, 1990.

[4] D.J. Elliot, B.P. Piwczyk, Single and multiple pulse ablation of polymeric and high density materials with excimer laser radiation at 193 nm and 248 nm. Mater. Res. Soc. Symp. Proc. vol. 129, Materials Research Society, Pittsburgh, 1989, pp. 627–636.

[5] C. P. Grigoropoulos, Heat transfer in laser processing of thin films, in: C.L. Tien (Eds.), Annual Review of Heat Transfer, vol. 5, Hemisphere, New York, 1994, pp. 77–130.

[6] J. Narayan, V.P. Gosbole, G.W. White, Laser method for synthesis and processing of continuous diamond films on nondiamond substrates, Science 52 (1991) 416–418.

[7] H.E. Elsayed-Ali, T.B. Norris, M.A. Pessot, G.A. Mourou, Time-resolved observation of electron–phonon relaxation in copper, Phys. Rev. Lett. 58 (1987) 1212–1215.

[8] S.D. Brorson, J.G. Fujimoto, E.P. Ippen, Femtosecond electron heat-transport dynamics in thin gold film, Phys. Rev. Lett. 59 (1987) 1962–1965.

[9] T.Q. Qiu, C.L. Tien, Short-pulse laser heating on metals, Int. J. Heat Mass Transfer 35 (1992) 719–726.

[10] T.Q. Qiu, C.L. Tien, Heat transfer mechanisms during short-pulse laser heating of metals, ASME J. Heat Transfer 115 (1993) 835–841.

[11] T.Q. Qiu, C.L. Tien, Femtosecond laser heating of multi-layered metals – I. Analysis, Int. J. Heat Mass Transfer 37 (1994) 2789–2797.

[12] T.Q. Qiu, T. Juhasz, C. Suarez, W.E. Bron, C.L. Tien, Femtosecond laser heating of multi-layered metals – II. Experiments, Int. J. Heat Mass Transfer 37 (1994) 2799–2808.

[13] M.I. Kaganov, I.M. Lifshitz, M.V. Tanatarov, Relaxation between electrons and crystalline lattices, Sov. Phys. JETP 4 (1957) 173–178.

[14] S.I. Anisimov, B.L. Kapeliovich, T.L. Perel'man, Electron emission from metal surfaces exposed to ultra-short laser pulses, Sov. Phys. JETP 39 (1974) 375–377.

[15] D.Y. Tzou, A unified field approach for heat conduction from micro- to macro-scales, ASME J. Heat Transfer 117 (1995) 8–16.

[16] D.Y. Tzou, The generalized lagging response in small-scale and high-rate heating, Int. J. Heat Mass Transfer 38 (1995) 3231–3240.

[17] D.Y. Tzou, Experimental support for the lagging response in heat propagation, AIAA J. Thermophysics Heat Transfer 9 (1995) 686–693.

[18] D.Y. Tzou, Macro- to Micro-scale Heat Transfer: The Lagging Behavior, Taylor & Francis, Washington, DC, 1997.

[19] D.Y. Tzou, Ultrafast heat transport: the lagging behavior, in: Giga- to Terahertz Photonics, SPIE's 44th Annual Meeting and Exhibition, 18–23 July, Denver, Colorado, 1999 (invited paper).

[20] R.A. Guyer, J.A. Krumhansl, Solution of the linearized Boltzmann equation, Phys. Rev. 148 (1966) 766–778.
[21] M.E. Gurtin, A.C. Pipkin, A general theory of heat conduction with finite wave speeds, Arch. Ration. Mech. Anal. 31 (1968) 113–126.
[22] D.Y. Tzou, J.K. Chen, Thermal lagging in random media, AIAA J. Thermophysics Heat Transfer 12 (1998) 567–574.
[23] C. Cattaneo, A form of heat conduction equation which eliminates the paradox of instantaneous propagation, Comp. Rend. 247 (1958) 431–433.
[24] P. Vernotte, Some possible complications in the phenomena of thermal conduction, Comp. Rend. 252 (1961) 2190–2191.
[25] J. Casas-Vázquez, D. Jou, Nonequilibrium temperature versus local-equilibrium temperature, Phys. Rev. E 49 (1994) 1040–1048.
[26] K.S. Chiu, Temperature dependent properties and micro-void in thermal lagging, Ph.D. Dissertation, University of Missouri-Columbia, Columbia, Missouri, 1999.
[27] W.H. Press, S.A. Teukolsky, W.T. Vetterling, B.P. Flannery, Numerical Recipes, Cambridge University Press, New York, 1992.
[28] H.R.B. Orlande, M.N. Özisik, D.Y. Tzou, Inverse analysis for estimating the electron–phonon coupling factor in thin metal films, J. Appl. Phys. 78 (1995) 1843–1849.